

Dynamic phase transition into a mixed-CDW state in 1T-TaS₂ via a thermal quench

A. de la Torre,^{1,2,3,*} Q. Wang,³ B. Campbell,⁴ J. V. Riffle,⁴ D.

Balasundaram,^{5,6} P.M.Vora,^{5,6} J.P.C. Ruff,⁷ S. M. Hollen,⁴ and K. W. Plumb^{3,†}

¹*Quantum Materials and Sensing Institute, Northeastern University, Burlington, Massachusetts, 01803, USA*

²*Department of Physics, Northeastern University, Boston, Massachusetts, 02115, USA*

³*Department of Physics, Brown University, Providence, Rhode Island 02912, United States*

⁴*Department of Physics and Astronomy, University of New Hampshire, Durham, NH 03824*

⁵*Department of Physics and Astronomy, George Mason University, Fairfax, VA, 22030 USA*

⁶*Quantum Science and Engineering Center, George Mason University, Fairfax, VA, 22030 USA*

⁷*Cornell High Energy Synchrotron Source, Cornell University, Ithaca, NY, 14853, USA*

(Dated: July 12, 2024)

Ultrafast light-matter interaction has emerged as a new mechanism to exert control over the macroscopic properties of quantum materials toward novel functionality. To date, technological applications of these non-thermal phases are limited by their ultrashort lifetimes and low-ordering temperatures. Among the most studied photoinduced metastable phases for their technological promise is the hidden metallic charge density wave (H-CDW) in the model correlated CDW compound 1T-TaS₂. Despite active study and engineering, the nature of the photoinduced H-CDW remains the subject of debate and is only accessible at cryogenic temperatures. Here, we stabilize the H-CDW phase at thermal equilibrium up to near-room temperature by accessing an intermediate mixed CDW order regime via thermal quenching. Using x-ray high dynamic range reciprocal space mapping (HDRM) and scanning tunneling spectroscopy (STS), we reveal the coexistence of commensurate (C) CDW and H-CDW domains below 180 K during cooling and below 210 K during warming. Our findings show that each order parameter breaks basal plane mirror symmetry with different chiral orientations and induces out-of-plane unit cell tripling in the H-CDW phase. Despite metallic domain walls and a finite density of states at zero bias observed via STS, bulk resistance remains insulating due to CDW stacking disorder. This study establishes the H-CDW as a thermally stable phase and introduces a new mechanism for switchable metallic behavior in thin flakes of 1T-TaS₂ and similar materials with competing order phases.

INTRODUCTION

The correlated van der Waal material 1T-TaS₂ displays a series of first-order phase transitions associated with the onset of CDW orders with different degrees of commensurability [1–3]. First, at $T = 550$ K, a

mirror-symmetry preserving incommensurate (I) CDW onsets from a metallic high-temperature state [4]. At $T_{I-NC} \approx 350$ K, 1T-TaS₂ enters into a nearly commensurate (NC) CDW phase. The atomic rearrangement associated with the incommensurate NC-CDW (in-plane ordering wavevector $q_{||} = 0.284$ r.l.u.) leads to disconnected regions displaying a $\sqrt{13} \times \sqrt{13}$ structural reconstruction in which twelve Ta atoms move towards a central one forming a star-of-David (SOD) pattern [5]. The NC-CDW breaks the mirror plane symmetries of the lattice basal plane and spontaneously selects one of two chiral domains rotated from the a -axis by $\phi \approx 12^\circ$. Then, at $T_{NC-C} \approx 175$ K in cooling and $T_{NC-C} \approx 225$ K in warming, a 3D CDW order emerges from the NC-CDW phase. This low-temperature phase is commensurate (C) with the atomic lattice in-plane ($\phi = 13.9^\circ$ and $q_{||} = 0.277$ r.l.u.) with the in-plane C-CDW atomic reconstruction inheriting the chiral structure from the NC-CDW. On the other hand, in the out-of-plane direction, the C-CDW displays a large stacking disorder between dimerized CDW planes [1, 2].

In general, experimental probes spanning a large range of lengthscales find that 1T-TaS₂ samples lack domain twinning that is expected across a first-order phase transition [6–10]. This reflects the kinetics of the first cooling across the only first-order phase transition in 1T-TaS₂ that breaks in-plane mirror symmetries, T_{I-NC} [11, 12]. During synthesis, the 1T phase is stabilized by quenching to $T \approx 273$ K across the polytype transition, $T_{1T-2H} = 600$ K [1]. During this initial quench, the cooling rate across T_{I-NC} is effectively slow when compared to the intrinsic timescales of the electronic (\approx fs) and atomic (\approx ps) degrees of freedom and enables the nucleation of large chiral CDW domains with lateral sizes comparable to the correlation length of the order parameter [13]. The chiral domain structure of the C-CDW in 1T-TaS₂ is stable to cooling through T_{NC-C} [6–10] with suggestions that strain fields and defects can pin a single chirality [6, 14]. Still, chirality reversal of single domain samples has been demonstrated by repeated cleaving of a bulk sample [7] or by cycling through T_{I-NC} [15]. On the other hand, multi-chiral domain samples

can be engineered in thin exfoliated flakes by heating and quenching above T_{1T-2H} [16, 17] or upon irradiation with 800 nm laser pulses with fluence $F > 7 \text{ mJ/cm}^2$ [6]. Once created, chiral domain walls are long-lived at low temperatures, but a dominant chiral domain of dimensions comparable to the sample size can be restored by heating above T_{I-NC} and adiabatically cooling through the mirror symmetry-breaking IC-NC transition [6, 16, 17]. Thus, T_{I-NC} emerges as the relevant energy scale for chiral CDW domain nucleation in $1T\text{-TaS}_2$ as the initial mirror-symmetry breaking transition in the CDW phase diagram [1]. Moreover, x-ray pair distribution function has revealed that the in-plane Ta average displacement from the mean crystallographic position, a measure of the CDW formation, remains constant across the NC-C CDW transition. At the same time, it dramatically changes across T_{I-NC} [18].

An additional low-temperature metastable metallic CDW phase, the so-called hidden H-CDW phase, has been accessed in $1T\text{-TaS}_2$ from the insulating C-CDW state via a single femtosecond laser pulse of fluence larger than a critical value ($F_c > 1 \text{ mJ/cm}^2$) [19–21] or by exciting $1T\text{-TaS}_2$ with a ns voltage pulse [22–26]. The H-CDW phase locally resembles the SOD arrangement but breaks the large C-CDW domains into many nanoscale domains and has a metallic density of states [23, 27, 28]. These domains maintain the chirality of the C-CDW [19] and are related by a relative translation of the SOD pattern by a finite number of atomic lattice vectors [23, 27, 29]. Moreover, slight differences between the displacement of the Ta atoms between the H-CDW and the C-CDW distinguish the two. The H-CDW phases result in CDW Bragg peaks rotated by $\phi = 11.9^\circ$ from the a^* -axis with a larger basal plane ordering wavevector, $q_{||} = 0.284 \text{ r.l.u.}$. The CDW plane stacking also rearranges towards a $l = 1/3$ periodicity along the c-axis [19]. We note that a similar metallic mosaic state can also be induced by cooling thin exfoliated samples ($d < 24 \text{ nm}$) across T_{I-NC} with a cooling rate faster than 0.2 K/s [30] or by intrinsic strain and defect effects [31–33].

Despite much study, the origin of the H-CDW state remains controversial, with photodoping [27, 34], incoherent thermal effects [23, 35] or electron-phonon relaxation bottlenecks [28, 36] all possible explanations. Nonetheless, the H-CDW has attracted much interest, not only as an example of the non-thermal control of quantum materials [37] but also as a platform for new functional devices [38–40]. However, the H-CDW has only been stabilized for ultrashort periods ($100\mu\text{s}$) at temperatures above $T = 50 \text{ K}$ [20, 28, 41] preventing its deployment in efficient and fast memory devices towards novel technological applications [42].

Here, we demonstrate that the H-CDW phase exists at thermal equilibrium in $1T\text{-TaS}_2$ and extend its thermal stability to near-room temperature by accessing a new long-lived mixed-CDW state via a reversible ther-

mal quench across T_{I-NC} . We deploy x-ray high dynamic range reciprocal space mapping (HDRM) to unequivocally demonstrate the co-existence of the C-CDW and H-CDW states in thermally quenched samples. Each CDW order parameter is linked to a mirror-symmetry breaking chiral domain. The mixed-CDW state emerges from a multi-domain NC-CDW state below $T^{CD} = 180 \text{ K}$ in cooling and $T^{WU} = 210 \text{ K}$ in warming. The mixed-CDW remains stable up to T_{I-NC} . Scanning tunneling spectroscopy (STS) shows that the mixed-CDW is characterized by a semi-metallic in-plane density of states. At the same time, bulk resistivity remains insulating due to out-of-plane CDW stacking disorder in mixed CDW bulk samples. Our results demonstrate a new state in the phase diagram of $1T\text{-TaS}_2$, enabling a new mechanism to engineer a semimetallic density of states at near room temperature.

RESULTS

Accessing a novel mixed-CDW state by quenching through the mirror symmetry breaking transition. In Figure 1 **a**, we show a characteristic [HK0] plane reciprocal space map for the C-CDW phase of $1T\text{-TaS}_2$, collected after a standard cooling cycle. Red circular markers highlight the CDW reflections at $q_1^C = (\sigma_1^C, \sigma_2^C, l)$ and $q_2^H = (-\sigma_2^C, \sigma_1^C + \sigma_2^C, l)$ with $\sigma_1^C = 3/13 \text{ r.l.u}$ and $\sigma_2^C = 1/13 \text{ r.l.u}$ [1, 2], corresponding to a single C-CDW chiral domain. Additional non-indexable reflections in the reciprocal space map are attributed to a second small crystallite in our sample. Identical reciprocal space maps were obtained across many cooling cycles and samples. However, we found that the C-CDW domain structure depends on the cooling rate, and a fast thermal quench across T_{I-NC} can consistently produce a multi-domain CDW. Fig. 1 **b** shows the [HK0] reciprocal space map after an in-situ quench in our bulk sample across T_{I-NC} down to $T = 140 \text{ K}$ at a rate of 0.2 K/ms near T_{I-NC} (See Methods for a description of the in-situ quench method and calculation of quenching rates using heat diffusion calculations). We found that thermal quenching consistently resulted in a new set of superlattice reflections of opposite chirality to the original set of satellite peaks ($\phi = -12.3^\circ$) [Fig. 1 **b**]. The superior reciprocal space resolution of synchrotron single crystal HDRM enables us to resolve differences in the wavevector of the two sets of CDW Bragg peaks with different chirality. The in-plane wavevector magnitude $|q_{||}| = 0.284(3) \text{ \AA}^{-1}$ of the quenched-induced satellite peaks is larger than that of the C-CDW ($|q_{||}| = 0.277(3) \text{ \AA}^{-1}$) and agrees with that of the light-stabilized H-CDW state [19]. This is shown in Fig. 1 **c**, where we display the integrated intensity across the C-CDW and H-CDW Bragg peaks (dashed lines in Fig. 1 **a** and **b**) as a function of $|q_{||}|$. Strikingly, each order parameter preferentially selects a chirality orienta-

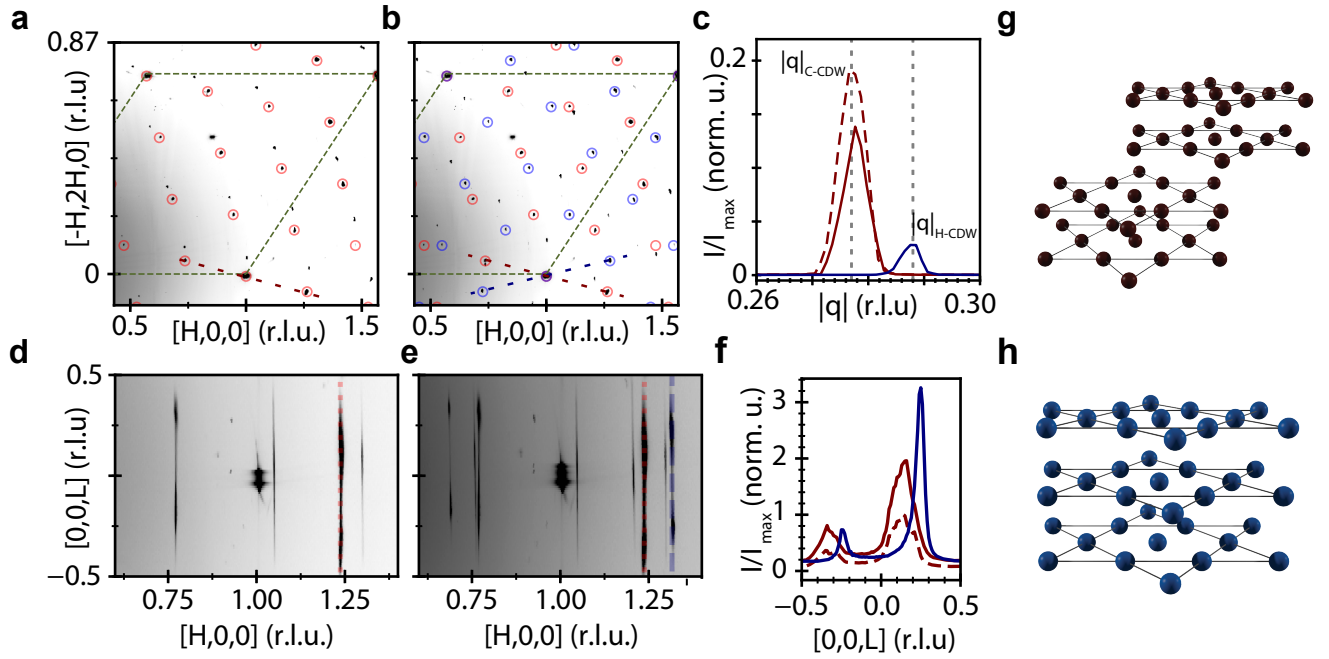


FIG. 1. Thermal quench into the mixed-CDW phase. **a.** Reciprocal space maps parallel to the [HK0] plane ($\delta L=.5$, $L=0$) at $T=140$ K for an as-grown sample. **b.** Reciprocal space maps parallel to the [HK0] plane ($\delta L=.5$, $L=0$) at $T=80$ K after a quench. Red and blue markers highlight the C-CDW and H-CDW-like satellite peaks, respectively. Green dashed lines highlight the a^* and b^* directions. **c** Average intensity dependence as a function of $|q|$ across a C-CDW satellite peak in the as-grown sample (dashed red line) and the C-CDW (red line) and H-CDW-like (blue line) after a quench. (Red and blue dashed lines in **b**). Vertical dashed lines correspond to the reported $|q_{||}|$ values for the C-CDW [1] and H-CDW [19] satellite peaks. **d** Reciprocal space map parallel to the [H0L] plane for the as-grown sample. **e** Reciprocal space map parallel to the [H0L] plane for the quenched sample. Vertical red and blue dashed lines indicate C-CDW and H-CDW-like satellite peaks, respectively. **f** Integrated intensity along [h0L] for the as-grown sample (red dashed) and after a quench (red, C-CDW peak and blue, H-CDW peak). **g** Schematic of the CDW dimerization in the as-grown sample. **h** Schematic of the $l=1/3$ CDW order in the H-CDW phase.

tion, with the C-CDW domains of the mixed-CDW phase maintaining that of the as-grown samples.

We also find that the c-axis periodicity differs between the C-CDW and H-CDW-like domains. Figure 1 **d** and **e** show [H0L] reciprocal space maps centered at $H=1$ r.l.u and $L=0$ r.l.u before and after the thermal quench, respectively. The as-grown sample displays a broad two-peak structure, with the center of mass at integer values of L . These short-range out-of-plane correlations are characteristic of the dimerization of CDW layers in the low-temperature C-CDW phase (Fig. 1 **g**) [43]. On the other hand, the H-CDW-like satellite peaks shift towards $l=\pm 1/3$ indicating a collapse of the interlayer dimerization towards a triple layer CDW stacking (Fig. 1 **h**) as was observed for the light-induced H-CDW [19]. The H-CDW-like satellite peaks are sharper than the C-CDW ones, reflecting a longer correlation length for the quench-induced domains $\xi=6(6)$ nm (Fig. 1 **f**). Our HDRM data in quenched samples demonstrates the coexistence of the C-CDW with a second CDW phase with the same order parameter as the H-CDW phase at much higher temperatures ($T=140$ K).

Critical temperature and metastability of the quenched mixed-CDW state. We performed a set of in-situ thermal cycles to directly demonstrate that (i) T_{I-NC} is the relevant temperature scale to access the mixed state and (ii) the transition is reversible. Consecutive thermal quenches were performed at different quench rates and starting temperatures, as illustrated in Figure 2 **a** (see Methods and Extended data). We found that after quenching from above T_{I-NC} , the mixed CDW state is thermally stable and insensitive to warming-cooling cycles if temperature kept less than T_{I-NC} [Fig. 2 **b**]. Such thermal stability is in contrast with the light-induced H-CDW phase that was found to be suppressed above $T=60$ K [20]. However, the C-CDW state can be recovered from the mixed state by warming up and slow-cooling across T_{I-NC} (Fig. 2 **c**). Subsequent thermal quenches from $T=300$ K do not recover the mixed state (Fig. 2 **d**), which can only be recovered upon heating and quenching from above T_{I-NC} (Fig. 2 **e**). Thus, our data confirms the IC-NC CDW as the necessary energy scale to access the mixed-CDW phase containing both the C-CDW and H-CDW order parameters.

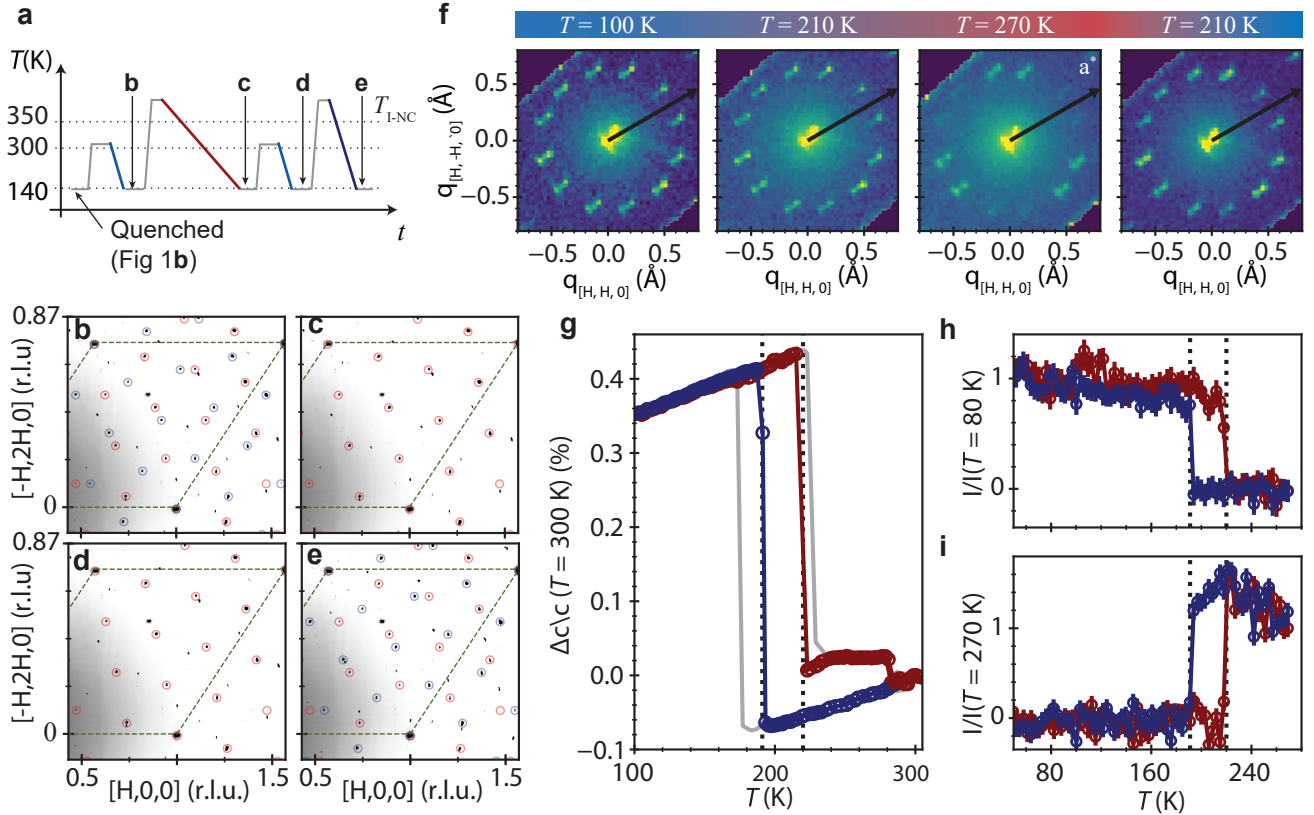


FIG. 2. Temperature dependence of the mixed-CDW. **a** Schematic of the subsequent in-situ thermal cycles undergone by a pre-quenched sample. **b-e** HRDM reciprocal space maps parallel to $[HK0]$ plane ($\delta L = .5$, $L = 0$) at $T = 140$ K after a thermal cycle as indicated in **a**. Red and blue markers highlight the C-CDW and H-CDW-like satellite peaks. Green dashed lines highlight the a^* and b^* directions. **f** Ag K_α reciprocal space maps parallel to the $[HK0]$ ($\delta L = .5$, $L = 10$) as a function of temperature across the C-NC transition. The black arrow encodes the a^* direction. **g** Temperature dependence of the relative change of the c -axis lattice parameter during cooling (blue) and heating (red) for a quenched sample (circular markers). Grey solid lines showcase the same magnitude for an as-grown sample. The quenched crystal shows a narrow hysteresis window for the C-NC transition compared to an as-grown sample. **h** Temperature dependence of a H-CDW-like satellite peak ($L = 9.66, \delta L = .1$) during cooling (blue) and warming (red). The thermal hysteresis follows that of the c -axis. **i** Temperature dependence of a H-CDW-like-precursor satellite peak ($L = 9.33, \delta L = .1$) in the NC phase during cooling (blue) and warming (red). Error bars in **h** and **i** represent one standard deviation.

The stability of the H-CDW phase at temperatures below T_{I-NC} in the mixed CDW phase enables us to ex-situ engineer the CDW mixed state at high temperatures (see Methods). We note that the mixed CDW state is stable over months, independent of the number of cleaves, and has been reproduced in quenched samples over multiple growth batches. Detailed temperature-dependent XRD measurements (See Methods) are shown in Fig. 2 f. All ex-situ quenched samples display twelve satellite reflections characteristic of the mixed-CDW state at low temperatures. Upon warming above $T^{WU} = 210$ K, or cooling below $T^{CD} = 195$ K, we observe a transition into an NC-CDW state with CDW Bragg peaks of two opposite chiralities. The existence of two chiral states in the NC-CDW is consistent with previous ultrafast electron diffraction experiments in $1T$ -TaS₂ driven with a low fluence optical pump reporting that the chirality of the

low-temperature C-CDW domains is inherited from the symmetry-breaking IC-NC transition [44]. We remark that this is distinct from the metastable H-CDW phase, which directly emerges from the C-CDW while maintaining the same chirality [19, 20, 27]. Detailed temperature dependence of the H-CDW-like peak and its NC-CDW precursor are shown in Fig. 2 h and i. C-CDW and H-CDW-like Bragg peaks show the same temperature dependence (see Extended data) suggesting the coupled nature of the two order parameters in the mixed-CDW phase. The asymmetrically narrower hysteretic loop of the first-order transition, when compared to as-grown samples, $T^{CD} = 180$ K and $T^{WU} = 210$ K, in conjunction with the narrower CDW Bragg peaks along L and the temperature dependence of the $[0010]$ structural Bragg peak shown in Fig. 2 c, suggests longer range interlayer ordering and a more 3D nature of the H-CDW phase.

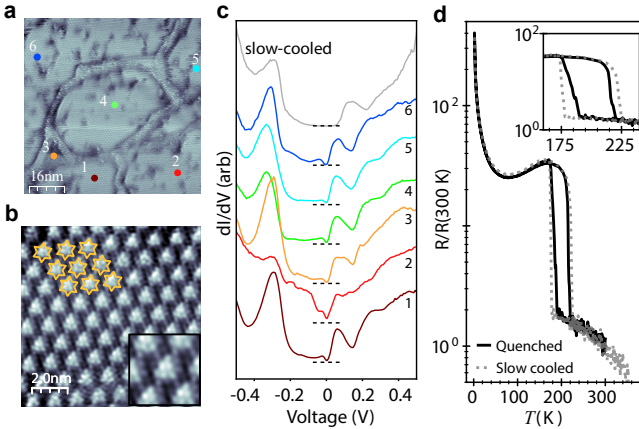


FIG. 3. Electronic structure of the mixed-CDW phase
a - b Representative topography of the mixed-CDW phase showing domains, atomic resolution and the $\sqrt{13} \times \sqrt{13}$ reconstruction. **c** dI/dV curves at each of the 6 domains seen in **d**. dI/dV data reflects a narrower gap in the electronic structure of $1T\text{-TaS}_2$ compared to the slow-cooled C-CDW phase (grey). Metallic behavior is observed in domain walls as indicated by point 3. **d** Resistivity, normalized to that at $T=300$ K for a mixed-sample (solid line) and as-grown sample (dotted grey). The inset shows a zoom in view around the TH-CDW/C-CDW transition.

Scanning tunneling microscopy (STM), measurements confirm the multi-domain nature of our quenched samples. Figure 3 **a** shows a characteristic $80 \times 80 \text{ nm}^2$ area in a quenched sample. Each domain shows the atomic reconstruction of the sulfur layer due to low-temperature CDW, as shown in Fig. 3 **c** with $V=380 \text{ mV}$, $I=0.35 \text{ nA}$, scale bar length = 2 nm). We note that the in-plane momentum resolution of our STM experiments prevents us from distinguishing between the C-CDW and the H-CDW-like domains. However, from the Fourier transform of STM images with atomic resolution, we extract a rotated satellite peak $\phi = 12.8(5)^\circ$, that reflects the presence of domains of opposite chirality (See extended data).

To summarize, intermediate-quenched bulk $1T\text{-TaS}_2$ samples host a mixed CDW state with two distinct order parameters, locked to opposite chiral phases, which emerge from a multi-chiral NC-CDW phase. Moreover, our temperature-dependent data reveals the narrowing of the hysteretic window across the NC-mixed-CDW phase transition. This indicates a stronger out-of-plane electronic correlation in the mixed-CDW phase of $1T\text{-TaS}_2$.

Electronic structure of the bulk quenched samples. We now bring attention to the low-temperature electronic structure of the mixed-CDW phase. While the origin of the insulating nature of the C-CDW remains controversial [45, 46], it is well established that the c -axis stacking of CDW domains strongly influences the electronic structure of $1T\text{-TaS}_2$ [47–50]. Moreover, recent STM and scanning tunneling spectroscopy (STS)

studies of the stack shift between in-plane domains in consecutive layers have identified interlayer coupling as the key ingredient that determines the band structure of the low-temperature CDW phase in $1T\text{-TaS}_2$ [23, 27, 51–53]. Thus, we use STS to study the low-temperature electronic state of the quenched samples. dI/dV curves taken at $T=10 \text{ K}$ within six different domains, Fig. 3 **a**, reveal a reduction of the $E_g=300 \text{ meV}$ gap of the C-CDW [10] towards a state with a reduced but non-zero density of states at the Fermi level (Fig. 3 **c**). While a transition to a semimetallic state is consistent with that observed for the H-CDW [23, 27], the density of states maintains the two pronounced peaks at around $V_B = -300 \text{ meV}$ and $V_B = 150 \text{ meV}$, that have been associated with the lower and upper Hubbard bands [54–56]. Despite the finite in-plane density of states at E_F and the formation of metallic domain walls (Fig. 3 **b**, curve 3), electrical transport in the mixed-CDW sample resembles that of the as-grown crystals.

We observed that quenched bulk samples display insulating behavior at all temperatures with the same relative resistivity increase with respect to $R(300 \text{ K})$ as the C-CDW phase [1] (Figure 3 **d**). The mixed state resistivity exhibits a narrow thermal hysteresis that tracks that of the structural transition (Fig. 2 **g**), reflecting the role of out-of-plane order in the resistivity of $1T\text{-TaS}_2$. The insulating nature of the mixed-CDW phase is distinct from the substantial $T < 70 \text{ K}$ resistivity drop observed for the light-induced H-CDW phase in thin samples [20]. This difference likely originates from the insulating C-CDW domains that occupy a large volume fraction of the mixed-CDW state and stacking CDW disorder between the two CDW orders with different periodicity along L (Figure 2 **g-h**). Additionally, we find that in-situ thermal cycling above $T_{IC}=350 \text{ K}$ and slow cooling recovers the characteristic resistivity of bulk $1T\text{-TaS}_2$ with a hysteretical transition separated by $\Delta T=50 \text{ K}$ (Figure 3 **d**), consistent with our diffraction measurements in as-grown samples. Thus, our STS, resistivity, and XRD data support an interpretation in which bulk metallic transport is impeded by the stacking disorder along L of two order parameters with different long-range intralayer CDW order [57].

DISCUSSION

In summary, our results demonstrate that a mixed-CDW phase characterized by C-CDW and H-CDW domains of opposite chirality can be stabilized by a thermal quench through T_{1-NC} . Our STS data reveals a semimetallic in-plane electronic density of states, while out-of-plane CDW stacking disorder prevents bulk metallic behavior.

It is compelling to compare our observations with theories for first-order dynamical phase transitions with two

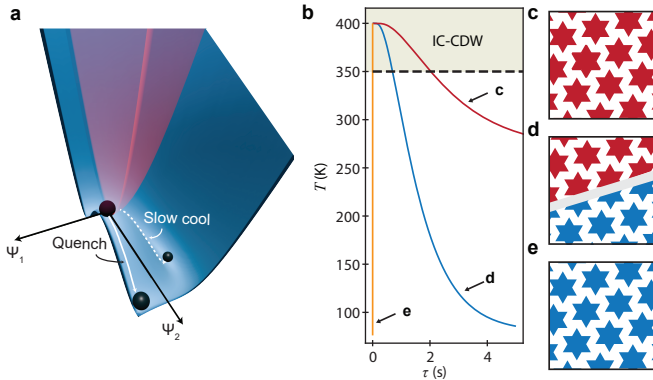


FIG. 4. Dynamic phase transition with two competing order parameters in 1T-TaS₂. **a** Schematic free energy landscape for a dynamical phase transition with two competing order parameters. A quench can stabilize a local minimum, different than the global minimum with order parameter ψ_1 , corresponding to a secondary order parameter ψ_2 . **b-d** Schematic of the possible low-temperature groundstates of 1T-TaS₂ as a function of quenching rate. **c** C-CDW, **d** mixed-CDW state and **e** H-CDW.

competing order parameters [58], in which the order parameter of the C-CDW corresponds to the global minimum of the free energy landscape. Under this hypothesis, the H-CDW phase is a local minimum of the free-energy landscape as sketched in Fig. 4 a. This provides a natural explanation for the large C-CDW domains for slow quenches, as sketched in Fig. 4 b and c. Such a free energy landscape allows a mixed inhomogeneous phase to be accessed at intermediate but adiabatic quenching rates in which a single temperature can be defined for all the different degrees of freedom in the material. This state is characterized by the coexistence of trapped regions of the two competing orders [59] and enhanced lifetime due to the transiently created domain walls [58]. Our data is consistent with such a scenario: in 1T-TaS₂ a thermal quench stabilizes a mixed phase of H-CDW and C-CDW order parameters up to $T = 180$ K in cooling and $T = 210$ K in warming (Fig. 4 d).

We note that all our thermal quenching attempts were unsuccessful in engineering a sample without signatures of the C-CDW state, as sketched in Fig. 4 e. It is likely that the quench protocol we describe here results in a nonuniform quench rate that is locally too slow over some regions of the sample to allow for the nucleation of the H-CDW domains. Within this context, previous ultrafast stabilization of the H-phase in thin flakes [19–26], can be understood as a non-thermal ultrafast quench [58]. Our results are consistent with proposals in which the absorption of energy by the electronic degrees of freedom suppresses the C-CDW order parameter. The consequent relaxation of the non-thermal electrons via the lattice leads to an ionic displacement from that of the C-CDW state into that of the H-CDW [28] allowing for

the correlations of the H-CDW order parameter to grow [58]. Thus, our results suggest that the minimum of the free energy landscape associated with the H-CDW order parameter already exists at the thermodynamic equilibrium of 1T-TaS₂ and can be accessed with a sufficiently fast adiabatic quench (Figure 3 a).

Our quenching protocol and the observation of the mixed-CDW phase opens a new pathway towards the development of new efficient functional devices based on 1T-TaS₂ in which H and C-CDW domain engineering can lead to switchable metallic behavior at temperatures above LN₂ [25, 38, 39]. More generally, our results have implications for the dynamic control of quantum materials [37, 60] by establishing that for macroscopic order parameters, the engineering of free energy landscapes can be achieved without the need for strong laser pulses when a thermally stable phase is already present at equilibrium [61–63].

DATA AVAILABILITY

The datasets obtained in this study are available in the open database at (To be provided).

ACKNOWLEDGEMENTS

A.d.l.T acknowledges helpful conversation with Michael Buchhold, Yue Cao, Martin Claassen, Greg Fiete, Simon Gerber, and Dante M. Kennes. Work performed at Brown University by A.d.l.T., Q.W. and K.W.P. was supported by the U.S. Department of Energy, Office of Science, Office of Basic Energy Sciences, under Award Number DE-SC0021223. P.M.V. and D.B. acknowledge support from NSF DMR 2226097 and the Mason Graduate Division's Presidential Scholarship Program". This work is based on research conducted at the Center for High-Energy X-ray Sciences (CHEXS), which is supported by the National Science Foundation (BIO, ENG and MPS Directorates) under award DMR-1829070.

AUTHOR CONTRIBUTIONS

A.d.l.T and Q. W. synthesized and characterized the single crystal samples. A.d.l.T., Q. W., K. W. P. and J.P.C.R. performed the High Dynamic Range x-ray scattering measurements. All x-ray experimental data was analyzed and interpreted by A.d.l.T and K .W. P.. B. C., J. V. R., and S. M. H. performed and analyzed the STM and STS measurements. D. B. and P.M.V. performed the cryo-Raman experiments. A.d.l.T. and K. W. P wrote the manuscript with input from all co-authors.

METHODS

Sample Growth

1T-TaS₂ bulk single crystals were grown by chemical vapor transport, with iodine as the transport agent. Stoichiometric amounts of elemental Ta and S were sealed in a quartz tube. The tubes were held at a 950° C – 850° C temperature gradient for 240 h and then placed in ice water to stabilize the 1T phase. Samples were characterized by XRD, resistivity, and Raman (see Fig. 2).

Thermal quench

Bulk 1T-TaS₂ crystals were sealed in a 1" quartz tube filled with Ar gas. The 1T-TaS₂ samples were then annealed by warming them up to 420 K, below the polytype transition at 660 K, with an 8h hold. This was followed by either a fast quench in which the quartz tube is dropped in a reservoir of LN₂ or slow cooling at room temperature. In-situ quench was performed at the QM2 beamline of the CHESS synchrotron by alternating between hot gas and a LN₂ cryo-stream.

Estimate of the cooling rate

To provide an estimate of the cooling rate for our 1T-TaS₂ sample quenched within an Ar-filled quartz ampule shown in Fig. 4 a and Extended data, we solve the heat diffusion equation for a system with cylindrical symmetry under the assumption that 1T-TaS₂ is at all times thermalized with the Ar bath and that the outside surface of the quartz tube is thermalized with the bath. Thus, the limiting factor to thermalization is the heat diffusion from the hot Ar volume at the starting temperature ($\rho_{Ar} = 1.8 \text{ kg/m}^3$, $K_{Ar} = 0.0179 \text{ W/(m}\cdot\text{K)}$, $C_p^{Ar} = 400 \text{ Jkg}^{-1}\text{m}$) through the 1.1 mm thick quartz wall with the outer surface acting as the heat sink ($\rho_Q = 2650 \text{ kg/m}^3$, $K_Q = 1$, $C_p^Q = 700 \text{ JKg}^{-1}\text{m}$)).

X-ray High Dynamic Range Reciprocal Space Mapping

Hard x-ray (20 keV) HDRM was performed at the QM2 beamline of Cornell High Energy Synchrotron Source (CHESS) using a Pilatus 6M area detector. The sample is mounted on a Kapton pin using GE varnish and rotated around three different axes by 360°. Data is collected at every 0.1° step with a frame rate of 0.1s. The data is reduced into a 3D stack, indexed, and projected into a 2D dataset using the beamline software.

In-house XRD measurements

In-house XRD measurements were performed on a Huber four-circle diffractometer in combination with a micro-focused Ag K_{α} x-ray source and a 256 x 256 pixel GaAs detector (pixel size 55 x 55 μm) situated 96 cm away from the center of rotation. Data was reduced using the same software as for the CHESS data.

STM/STS measurements

STM and STS measurements were performed on a RHK Technology PanScan Freedom closed-cycle STM. Samples for the STM/STS measurements were mounted on stainless steel post holders using conductive silver epoxy and quenched as previously described. After the quench, the samples were characterized by XRD and kept below $T = 370\text{K}$. The surface of a 1T-TaS₂ crystal was cleaved at room temperature and $\approx 10^{-10} \text{ mbar}$ by carbon tape and a cleaving screw before being introduced to the STM stage and cooled to 10 K. All data presented here were taken at 10 K.

Resistivity

Resistivity measurements were performed using a Quantum Design Physical Properties Measurement System (PPMS). Samples were mounted on a DC resistivity puck and a standard four-probe method was used, with Au wires and Ag paste contacts.

Raman Spectroscopy

Raman measurements of quenched and unquenched TaS₂ single crystals are performed at 5 K in a closed-cycle He cryostat. The samples are excited in a backscattering geometry with a 532 nm laser focused through a 0.6 NA objective lens with 40 \times magnification. The laser power was measured to be 110 μW before the objective. The scattered light was collected through the same lens and directed to an imaging spectrograph with a liquid nitrogen-cooled charge-coupled device. Rejection of the Rayleigh scattered light is accomplished using three-volume Bragg gratings that allow measurement of Raman photons down to 10 cm^{-1} .

* Corresponding author:a.delatorreduran@northeastern.edu

† Corresponding author:kemp.plumb@brown.edu

[1] A.H. Thompson, R.F. Gamble, and J.F. Revelli, "Transitions between semiconducting and metallic phases in 1-t tas2," Solid State Communications **9**, 981–985 (1971).

[2] J.A. Wilson, F.J. Di Salvo, and S. Mahajan, "Charge-density waves and superlattices in the metallic layered transition metal dichalcogenides," *Advances in Physics* **24**, 117–201 (1975).

[3] P Fazekas and E Tosatti, "Electrical, structural and magnetic properties of pure and doped 1t-tas₂," *Philosophical Magazine B* **39**, 229–244 (1979).

[4] B. Sipos, A. F. Kusmartseva, A. Akrap, H. Berger, L. Forró, and E. Tutiš, "From mott state to superconductivity in 1t-tas₂," *Nature Materials* **7**, 960–965 (2008).

[5] Albert Spijkerman, Jan L. de Boer, Auke Meetsma, Gerrit A. Wiegers, and Sander van Smaalen, "X-ray crystal-structure refinement of the nearly commensurate phase of 1t-tas₂ in (3+2)-dimensional superspace," *Phys. Rev. B* **56**, 13757–13767 (1997).

[6] Alfred Zong, Xiaozhe Shen, Anshul Kogar, Linda Ye, Carolyn Marks, Debanjan Chowdhury, Timm Rohwer, Byron Freelon, Stephen Weathersby, Renkai Li, Jie Yang, Joseph Checkelsky, Xijie Wang, and Nuh Gedik, "Ultrafast manipulation of mirror domain walls in a charge density wave," *Science Advances* **4**, eaau5501 (2018).

[7] Bryan T. Fichera, Anshul Kogar, Linda Ye, Bilal Gökce, Alfred Zong, Joseph G. Checkelsky, and Nuh Gedik, "Second harmonic generation as a probe of broken mirror symmetry," *Phys. Rev. B* **101**, 241106 (2020).

[8] Xiangpeng Luo, Dimuthu Obeysekera, Choongjae Won, Suk Hyun Sung, Noah Schnitzer, Robert Hovden, Sang-Wook Cheong, Junjie Yang, Kai Sun, and Liuyan Zhao, "Ultrafast modulations and detection of a ferro-rotational charge density wave using time-resolved electric quadrupole second harmonic generation," *Phys. Rev. Lett.* **127**, 126401 (2021).

[9] H. F. Yang, K. Y. He, J. Koo, S. W. Shen, S. H. Zhang, G. Liu, Y. Z. Liu, C. Chen, A. J. Liang, K. Huang, M. X. Wang, J. J. Gao, X. Luo, L. X. Yang, J. P. Liu, Y. P. Sun, S. C. Yan, B. H. Yan, Y. L. Chen, X. Xi, and Z. K. Liu, "Visualization of chiral electronic structure and anomalous optical response in a material with chiral charge density waves," *Phys. Rev. Lett.* **129**, 156401 (2022).

[10] B. Campbell, J. V. Riffle, A. de la Torre, Q. Wang, K. W. Plumb, and S. M. Hollen, "Nanoscale electronic inhomogeneities in 1t-tas₂," *Phys. Rev. Mater.* **8**, 034002 (2024).

[11] D. Sept and J. A. Tuszyński, "Inhomogeneous nucleation in first-order phase transitions," *Phys. Rev. E* **50**, 4906–4910 (1994).

[12] K Binder, "Theory of first-order phase transitions," *Reports on Progress in Physics* **50**, 783 (1987).

[13] David W. Oxtoby, "Nucleation of first-order phase transitions," *Accounts of Chemical Research* **31**, 91–97 (1998).

[14] Björn Salzmann, Elina Hujala, Catherine Witteveen, Baptiste Hildebrand, Helmuth Berger, Fabian O. von Rohr, Christopher W. Nicholson, and Claude Monney, "Observation of the metallic mosaic phase in 1t-TaS₂ at equilibrium," *Phys. Rev. Mater.* **7**, 064005 (2023).

[15] Yan Zhao, Zhengwei Nie, Hao Hong, Xia Qiu, Shiyi Han, Yue Yu, Mengxi Liu, Xiaohui Qiu, Kaihui Liu, Sheng Meng, Lianming Tong, and Jin Zhang, "Spectroscopic visualization and phase manipulation of chiral charge density waves in 1t-tas₂," *Nature Communications* **14**, 2223 (2023).

[16] Suk Hyun Sung, Noah Schnitzer, Steve Novakov, Ismail El Baggari, Xiangpeng Luo, Jiseok Gim, Nguyen M. Vu, Zidong Li, Todd H. Brintlinger, Yu Liu, Wenjian Lu, Yuping Sun, Parag B. Deotare, Kai Sun, Liuyan Zhao, Lena F. Kourkoutis, John T. Heron, and Robert Hovden, "Two-dimensional charge order stabilized in clean polytype heterostructures," *Nature Communications* **13**, 413 (2022).

[17] Samra Husremović, Berit H. Goodge, Matthew P. Erodić, Katherine Inzani, Alberto Mier, Stephanie M. Ribet, Karen C. Bustillo, Takashi Taniguchi, Kenji Watanabe, Colin Ophus, Sinéad M. Griffin, and D. Kwabena Bediako, "Encoding multistate charge order and chirality in endotaxial heterostructures," *Nature Communications* **14**, 6031 (2023).

[18] Emil S Bozin, M Abeykoon, S Conradson, Gianguido Baldinozzi, P Sutar, and D Mihailovic, "Crystallization of polarons through charge and spin ordering transitions in 1t-tas₂," *Nature Communications* **14**, 7055 (2023).

[19] Quirin Stahl, Maximilian Kusch, Florian Heinsch, Gaston Garbarino, Norman Kretzschmar, Kerstin Hanff, Kai Rossnagel, Jochen Geck, and Tobias Ritschel, "Collapse of layer dimerization in the photo-induced hidden state of 1t-tas₂," *Nature Communications* **11**, 1247 (2020).

[20] L. Stojchevska, I. Vaskivskyi, T. Mertelj, P. Kusar, D. Svetin, S. Brazovskii, and D. Mihailovic, "Ultrafast switching to a stable hidden quantum state in an electronic crystal," *Science* **344**, 177–180 (2014).

[21] Igor Vaskivskyi, Jan Gospodarc, Serguei Brazovskii, Damjan Svetin, Petra Sutar, Evgeny Goreshnik, Ian A. Mihailovic, Tomaz Mertelj, and Dragan Mihailovic, "Controlling the metal-to-insulator relaxation of the metastable hidden quantum state in 1t-tas₂," *Science Advances* **1**, e1500168 (2015).

[22] Matthew J Hollander, Yu Liu, Wen-Jian Lu, Li-Jun Li, Yu-Ping Sun, Joshua A Robinson, and Suman Datta, "Electrically driven reversible insulator–metal phase transition in 1t-tas₂," *Nano letters* **15**, 1861–1866 (2015).

[23] Ligu Ma, Cun Ye, Yijun Yu, Xiu Fang Lu, Xiaohai Niu, Sejoong Kim, Donglai Feng, David Tománek, Young-Woo Son, Xian Hui Chen, *et al.*, "A metallic mosaic phase and the origin of mott-insulating state in 1t-tas₂," *Nature communications* **7**, 10956 (2016).

[24] Doohee Cho, Sangmo Cheon, Ki-Seok Kim, Sung-Hoon Lee, Yong-Heum Cho, Sang-Wook Cheong, and Han Woong Yeom, "Nanoscale manipulation of the mott insulating state coupled to charge order in 1t-tas₂," *Nature communications* **7**, 10453 (2016).

[25] Rok Venturini, Anže Mraz, Igor Vaskivskyi, Yevhenii Vaskivskyi, Damjan Svetin, Tomáž Mertelj, Leon Pavlović, Jing Cheng, Genyu Chen, Priyanthi Amarasinghe, Syed B. Qadri, Sudhir B. Trivedi, Roman Sobolewski, and Dragan Mihailovic, "Ultraefficient resistance switching between charge ordered phases in 1T-TaS₂ with a single picosecond electrical pulse," *Applied Physics Letters* **120**, 253510 (2022).

[26] Adam W. Tsien, Robert Hovden, Dennis Wang, Young Duck Kim, Junichi Okamoto, Katherine A. Spoth, Yu Liu, Wenjian Lu, Yuping Sun, James C. Hone, Lena F. Kourkoutis, Philip Kim, and Abhay N. Pasupathy, "Structure and control of charge density waves in two-dimensional 1t-tas₂," *Proceedings of the National Academy of Sciences* **112**, 15054–15059 (2015).

[27] Yaroslav A. Gerasimenko, Petr Karpov, Igor Vaskivskyi, Serguei Brazovskii, and Dragan Mihailovic, "Intertwined chiral charge orders and topological stabilization of the

light-induced state of a prototypical transition metal dichalcogenide,” *npj Quantum Materials* **4**, 32 (2019).

[28] Julian Maklar, Jit Sarkar, Shuo Dong, Yaroslav A. Gerasimenko, Tommaso Pincelli, Samuel Beaulieu, Patrick S. Kirchmann, Jonathan A. Sobota, Shuolong Yang, Dominik Leuenberger, Robert G. Moore, Zhi-Xun Shen, Martin Wolf, Dragan Mihailovic, Ralph Ernstorfer, and Laurenz Rettig, “Coherent light control of a metastable hidden state,” *Science Advances* **9**, eadi4661 (2023).

[29] Jan Ravnik, Michele Diego, Yaroslav Gerasimenko, Yevhenii Vaskivskyi, Igor Vaskivskyi, Tomaz Mertelj, Jaka Vodeb, and Dragan Mihailovic, “A time-domain phase diagram of metastable states in a charge ordered quantum material,” *Nature communications* **12**, 2323 (2021).

[30] Masaro Yoshida, Ryuji Suzuki, Yijin Zhang, Masaki Nakano, and Yoshihiro Iwasa, “Memristive phase switching in two-dimensional 1t-tas₂ crystals,” *Science Advances* **1**, e1500606 (2015).

[31] H. Mutka, L. Zuppiroli, P. Molinié, and J. C. Bourgoin, “Charge-density waves and localization in electron-irradiated 1t-Tas₂,” *Phys. Rev. B* **23**, 5030–5037 (1981).

[32] Wenhao Zhang, Jingjing Gao, Li Cheng, Kunliang Bu, Zongxiu Wu, Ying Fei, Yuan Zheng, Li Wang, Fangsen Li, Xuan Luo, Zheng Liu, Yuping Sun, and Yi Yin, “Visualizing the evolution from mott insulator to anderson insulator in ti-doped 1t-tas₂,” *npj Quantum Materials* **7** (2022), 10.1038/s41535-021-00415-5.

[33] Björn Salzmann, Elina Hujala, Catherine Witteveen, Baptiste Hildebrand, Helmuth Berger, Fabian O. von Rohr, Christopher W. Nicholson, and Claude Monney, “Observation of the metallic mosaic phase in 1t-TaS₂ at equilibrium,” *Phys. Rev. Mater.* **7**, 064005 (2023).

[34] Kai Sun, Shuaishuai Sun, Chunhui Zhu, Huanfang Tian, Huaixin Yang, and Jianqi Li, “Hidden cdw states and insulator-to-metal transition after a pulsed femtosecond laser excitation in layered chalcogenide 1T-TaS_{2-x}Se_x,” *Science Advances* **4**, eaas9660 (2018).

[35] Frank Y. Gao, Zhuquan Zhang, Zhiyuan Sun, Linda Ye, Yu-Hsiang Cheng, Zi-Jie Liu, Joseph G. Checkelsky, Edoardo Baldini, and Keith A. Nelson, “Snapshots of a light-induced metastable hidden phase driven by the collapse of charge order,” *Science Advances* **8**, eabp9076 (2022).

[36] Pierre-Adrien Mante, Chin Shen Ong, Daniel Finkelstein Shapiro, Arkady Yartsev, Oscar Gränäs, and Olle Eriksson, “Photo-induced hidden phase of 1t-tas₂ with tunable lifetime,” (2022), arXiv:2203.13509 [cond-mat.mtrl-sci].

[37] Alberto de la Torre, Dante M. Kennes, Martin Claassen, Simon Gerber, James W. McIver, and Michael A. Sentef, “Colloquium: Nonthermal pathways to ultrafast control in quantum materials,” *Rev. Mod. Phys.* **93**, 041002 (2021).

[38] D. Mihailovic, D. Svetin, I. Vaskivskyi, R. Venturini, B. Lipovšek, and A. Mraz, “Ultrafast non-thermal and thermal switching in charge configuration memory devices based on 1T-TaS₂,” *Applied Physics Letters* **119**, 013106 (2021).

[39] Anze Mraz, Rok Venturini, Damjan Svetin, Vitomir Sever, Ian Aleksander Mihailovic, Igor Vaskivskyi, Bojan Ambrozic, Goran Dražić, Maria D’Antuono, Daniela Stornaiuolo, Francesco Tafuri, Dimitrios Kazazis, Jan Ravnik, Yasin Ekinci, and Dragan Mihailovic, “Charge configuration memory devices: Energy efficiency and switching speed,” *Nano Letters* **22**, 4814–4821 (2022).

[40] T. R. Devidas, Jonathan T. Reichanadter, Shannon C. Haley, Matan Sterenberg, Joel E. Moore, Jeffrey B. Neaton, James G. Analytis, Beena Kalisky, and Eran Maniv, “Spontaneous conducting boundary channels in 1t-tas₂,” (2024), arXiv:2405.02036 [cond-mat.str-el].

[41] Jan Ravnik, Igor Vaskivskyi, Tomaz Mertelj, and Dragan Mihailovic, “Real-time observation of the coherent transition to a metastable emergent state in 1t-tas₂,” *Physical Review B* **97**, 075304 (2018).

[42] DN Basov, RD Averitt, and D Hsieh, “Towards properties on demand in quantum materials,” *Nature materials* **16**, 1077–1088 (2017).

[43] Satoshi Tanda, Takashi Sambongi, Toshiro Tani, and Shoji Tanaka, “X-ray study of charge density wave structure in 1t-tas₂,” *Journal of the Physical Society of Japan* **53**, 476–479 (1984).

[44] Kerstin Haupt, Maximilian Eichberger, Nicolas Erasmus, Andrea Rohwer, Jure Demsar, Kai Rossnagel, and Heinrich Schwoerer, “Ultrafast metamorphosis of a complex charge-density wave,” *Phys. Rev. Lett.* **116**, 016402 (2016).

[45] Francesco Petocchi, Christopher W. Nicholson, Bjoern Salzmann, Diego Pasquier, Oleg V. Yazyev, Claude Monney, and Philipp Werner, “Mott versus hybridization gap in the low-temperature phase of 1t-tas₂,” *Phys. Rev. Lett.* **129**, 016402 (2022).

[46] Y. D. Wang, W. L. Yao, Z. M. Xin, T. T. Han, Z. G. Wang, L. Chen, C. Cai, Yuan Li, and Y. Zhang, “Band insulator to mott insulator transition in 1t-tas₂,” *Nature Communications* **11**, 4215 (2020).

[47] T. Ritschel, H. Berger, and J. Geck, “Stacking-driven gap formation in layered 1t-tas₂,” *Phys. Rev. B* **98**, 195134 (2018).

[48] Sung-Hoon Lee, Jung Suk Goh, and Doohee Cho, “Origin of the insulating phase and first-order metal-insulator transition in 1t-tas₂,” *Phys. Rev. Lett.* **122**, 106404 (2019).

[49] CJ Butler, Masaro Yoshida, Tetsuo Hanaguri, and Yoshihiro Iwasa, “Mottness versus unit-cell doubling as the driver of the insulating state in 1t-tas₂,” *Nature communications* **11**, 2477 (2020).

[50] T Ritschel, J Trinckauf, K Koepernik, B Büchner, M v Zimmermann, H Berger, YI Joe, P Abbamonte, and J Geck, “Orbital textures and charge density waves in transition metal dichalcogenides,” *Nature physics* **11**, 328–331 (2015).

[51] Doohee Cho, Gyeongcheol Gye, Jinwon Lee, Sung-Hoon Lee, Lihai Wang, Sang-Wook Cheong, and Han Woong Yeom, “Correlated electronic states at domain walls of a mott-charge-density-wave insulator 1t-tas₂,” *Nature communications* **8**, 392 (2017).

[52] Jae Whan Park, Jinwon Lee, and Han Woong Yeom, “Zoology of domain walls in quasi-2d correlated charge density wave of 1t-tas₂,” *npj Quantum Materials* **6**, 32 (2021).

[53] Jae Whan Park, Jinwon Lee, and Han Woong Yeom, “Stacking and spin order in a van der waals mott insulator 1t-tas₂,” *Communications Materials* **4**, 99 (2023).

[54] L. Perfetti, T. A. Gloor, F. Mila, H. Berger, and M. Grioni, “Unexpected periodicity in the quasi-two-dimensional mott insulator 1t-tas₂ revealed by angle-resolved photoemission,” *Phys. Rev. B* **71**, 153101

(2005).

[55] Ju-Jin Kim, W. Yamaguchi, T. Hasegawa, and K. Kitazawa, "Observation of mott localization gap using low temperature scanning tunneling spectroscopy in commensurate $1t$ – Tas_2 ," Phys. Rev. Lett. **73**, 2103–2106 (1994).

[56] Doohee Cho, Yong-Heum Cho, Sang-Wook Cheong, Ki-Seok Kim, and Han Woong Yeom, "Interplay of electron-electron and electron-phonon interactions in the low-temperature phase of $1t$ – Tas_2 ," Phys. Rev. B **92**, 085132 (2015).

[57] Junde Liu, Pei Liu, Liu Yang, Sung-Hoon Lee, Mojun Pan, Famin Chen, Jierui Huang, Bei Jiang, Mingzhe Hu, Yuchong Zhang, Zhaoyang Xie, Gang Wang, Mengxue Guan, Wei Jiang, Huaixin Yang, Jianqi Li, Chenxia Yun, Zhiwei Wang, Sheng Meng, Yugui Yao, Tian Qian, and Xun Shi, "Nonvolatile optical control of interlayer stacking order in $1t$ - Tas_2 ," (2024), arXiv:2405.02831 [cond-mat.mtrl-sci].

[58] Zhiyuan Sun and Andrew J. Millis, "Transient trapping into metastable states in systems with competing orders," Phys. Rev. X **10**, 021028 (2020).

[59] Lorenzo Del Re, Michele Fabrizio, and Erio Tosatti, "Nonequilibrium and nonhomogeneous phenomena around a first-order quantum phase transition," Phys. Rev. B **93**, 125131 (2016).

[60] Giacomo Jarc, Shahla Yasmin Mathengattil, Angela Montanaro, Francesca Giusti, Enrico Maria Rigoni, Rudi Sergo, Francesca Fassioli, Stephan Winnerl, Simone Dal Zilio, Dragan Mihailovic, *et al.*, "Cavity-mediated thermal control of metal-to-insulator transition in $1t$ - Tas_2 ," Nature **622**, 487–492 (2023).

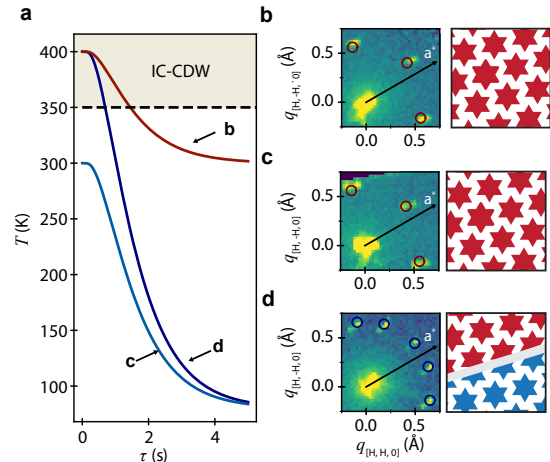
[61] Anushya Chandran, Amir Erez, Steven S. Gubser, and S. L. Sondhi, "Kibble-zurek problem: Universality and the scaling limit," Phys. Rev. B **86**, 064304 (2012).

[62] Kai Du, Xiaochen Fang, Choongjae Won, Chandan De, Fei-Ting Huang, Wenqian Xu, Hoydoo You, Fernando J. Gómez-Ruiz, Adolfo del Campo, and Sang-Wook Cheong, "Kibble-zurek mechanism of ising domains," Nature Physics (2023), 10.1038/s41567-023-02112-5.

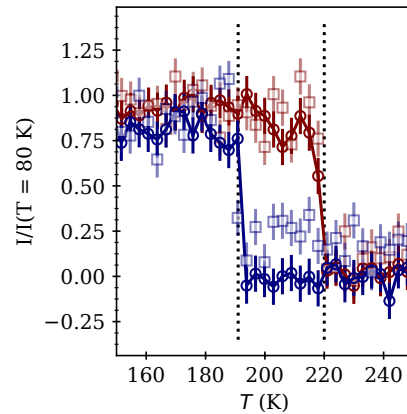
[63] Han Wu, Lei Chen, Paul Malinowski, Bo Gyu Jang, Qinwen Deng, Kirsty Scott, Jianwei Huang, Jacob P. C. Ruff, Yu He, Xiang Chen, Chaowei Hu, Ziqin Yue, Ji Seop Oh, Xiaokun Teng, Yucheng Guo, Mason Klemm, Chuqiao Shi, Yue Shi, Chandan Setty, Tyler Werner, Makoto Hashimoto, Donghui Lu, Turgut Yilmaz, Elio Vescovo, Sung-Kwan Mo, Alexei Fedorov, Jonathan D. Denlinger, Yaofeng Xie, Bin Gao, Junichiro Kono, Pengcheng Dai, Yimo Han, Xiaodong Xu, Robert J. Birgeneau, Jian-Xin Zhu, Eduardo H. da Silva Neto, Liang Wu, Jiun-Haw Chu, Qimiao Si, and Ming Yi, "Reversible non-volatile electronic switching in a near-room-temperature van der waals ferromagnet," Nature Communications **15** (2024),

10.1038/s41467-024-46862-z.

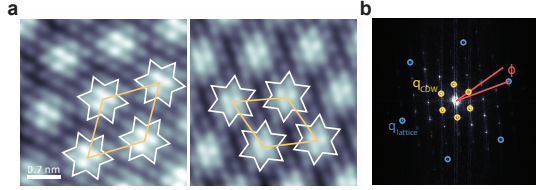
EXTENDED DATA



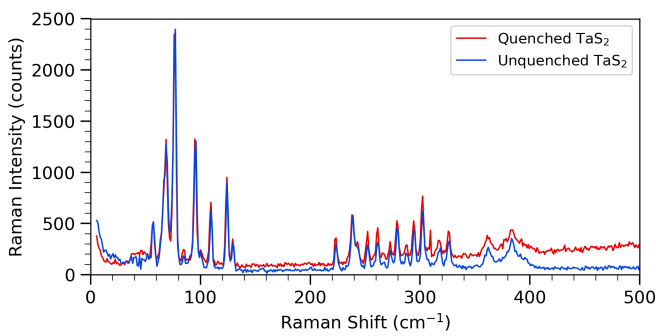
Extended Data 1. **a** Cooling rate simulations and reciprocal space maps and CDW state schematic **b-d** for three different scenarios: **b** slow cool from 400 K, **c** quench from 300 K and **d** quench from 400 K. Only the third case shown in **d** results in the emergence of the mixed CDW state.



Extended Data 2. Circular and square markers show the temperature dependence in cooling (blue) and warming (red) of two CDW Bragg peaks of opposite chirality in quenched samples of $1T$ - TaS_2 .



Extended Data 3. **a** STM data with atomic resolution in two domains with different chirality in Fig. 3**b**. **b** The high-intensity fundamental peaks ($q_{lattice}$) are highlighted in blue. The satellite peaks (q_{CDW} , yellow) are associated with the TH-CDW phase. The resolution of our STM measurements prevents us from resolving the difference in the magnitude and in-plane rotation of $|q|$ between the C-CDW and H-CDW.



Extended Data 4. Unpolarized Raman spectra in a quenched (red) and as-grown (blue) at $T=5$ K.